



Full Length Article

Pattern recognition for measuring the flame stability of gas-fired combustion based on the image processing technology



Yu Wang, Yuefeng Yu*, Xiaolei Zhu, Zhongxiao Zhang

School of Mechanical Engineering, Shanghai Jiao Tong University, Shanghai 200240, People's Republic of China

ARTICLE INFO

Keywords:

Combustion diagnosis
Gas-fired flame
Logarithmic entropy multi-threshold segmentation
Fuzzy pattern recognition
 Q and T^2

ABSTRACT

This study proposes a diagnostic method for gas-fired combustion based on the image processing technology, for identifying an abnormal combustion situation in a gaseous flame. The proposed algorithm is divided into four aspects: (1) a logarithmic entropy multi-threshold segmentation method for segmenting the flame region utilized to extract image features; (2) 12 typical characteristic parameters representing gas-fired flame images, with five of them extracted for identification; (3) a fuzzy pattern recognition algorithm using an *S*-type membership function and a maximum-minimum distance function to distinguish between variable flame states; and (4) two statistics, Q and T^2 , used to evaluate the decision-making results of the fuzzy pattern recognition. The results are also compared to those from several other algorithms, including the self-organizing map, neural network, and support vector machine methods. The experimental results indicate that the proposed method has better performance in identifying different combustion situations in a gaseous flame and is superior to the other algorithms. Through a two-parameter adjustment, normal gas-fired combustion state can be accurately identified; for abnormal combustion, the prediction accuracy can become more than 90%. There can be a slight misjudgment; this may be owing to the relatively less training data for abnormal flame states.

1. Introduction

Industrial combustion diagnosis based on digital image processing technology is a popular research topic in the field of combustion diagnostics. In recent years, researchers have proposed diverse flame detection algorithms based on representative image features, to distinguish between variable combustion situations [1,2]. Unfortunately, the majority of flame image features are generally incapable to represent the intrinsic invariance of flame properties, owing to their dependence on the flame structure. Meanwhile, the occurrence of an abnormal flame state inevitably leads to the chaotic behavior of the relevant flame characteristics in the combustion process frequently [3–6]. If optimization algorithms with lower adaptability are employed simultaneously, it may result in incorrect judgments on a flame state under different combustion conditions. Therefore, it is indispensable to develop more distinctive features of flame images that are independent from the flame structure. There is also a need for a feasible method for diminishing the misclassification of each combustion situation.

Scholars have proposed various algorithms of flame detection by using digital image processing as a diagnostic tool for combustion, most of which are based on an artificial neural network (ANN), a support vector machine (SVM), or other methods [2]. Khan Muhammad et al.

[7] proposed a framework regarding early fire detection based on fine-tuning a convolutional neural network by using a surveillance camera. The framework successfully distinguished flame on/off condition, instead of predicting and assessing the combustion regime. Man Hyung Lee et al. [8] combined image processing technology and an ANN-based algorithm to classify combustion states in the furnace of boilers in a power generation plant. Their approach enabled the automatic burner controller to respond quickly and accurately to the moment when the flame is extinguished, thus guaranteeing the economy and safety of boiler operation. Although both methods can provide evidence for the existence of a flame, they cannot evaluate the quality of combustion and quantify the flame stability. Hence, Jiesheng Wang et al. [9] established a novel identification method for identifying pulverized coal combustion states by applying a kernel principal component analysis (KPCA) and learning vector quantization neural-network model. After creating the relationships between the known combustion state and characteristic parameters of a pulverized coal-fired flame, the unknown combustion state could be identified, thus providing reference for the identification of different flame types and on-line diagnosis for combustion.

An ANN-based algorithm can establish a relationship between image data and the particular combustion state reflected in a flame

* Corresponding author.

E-mail address: yfyu@sjtu.edu.cn (Y. Yu).

Nomenclature

f	the focal length of the camera
α	the equivalence ratio
G	the gray-level intensity
H	the log-entropy function
T^*	the optimal threshold vector
V^k	the current speed of the particle
X^k	the current position of the particle
P_{id}	the individual optimal position
P_{gd}	the group optimal position
r_1 and r_2	random numbers (0–1)
w	the inertial factor of PSO model
S_f	total flame area
Ω	the connectivity
Φ	the circularity
G_A	mean value of grayscale

σ	standard deviation of grayscale
E	the gray entropy
a, b, C_1 , and C_2	parameters in fuzzy model
η and k	hyper-parameters (0–1)
δ^2	the confidence limit of Q statistic
χ^2	the confidence limit of T^2 statistic
φ	the composite indicator of Q and T^2 statistic
ψ^2	the confidence limit of φ statistic
CCD	charge coupled device
LEMTS	the logarithmic entropy multi-threshold segmentation
ANN	artificial neural network
SVM	support vector machine
SOM	self-organizing map
PSO	particle swarm optimization
PCA	the principal component analysis
FPR	fuzzy pattern recognition

image. For this method to realize the classification of flame states, a non-linear function is supposed to be built through the connections between multiple layers of different neurons [10,11]. However, an ANN-based algorithm is often limited, as it cannot get flame image data under all combustion operating conditions. In some cases, the severe instability caused by falling into local optimum will also be exhibited by the output of ANN. In addition, they are more suitable for offline image processing than real-time online processing [12]. Thus, many scholars have proposed using an SVM algorithm instead of an ANN-based algorithm. The SVM can make a distinction between different flame states in small training samples, and its nonlinear mapping capability under Gauss-kernel function is not inferior to that of the ANN-based algorithms [13–15]. Tung Xuan Truong et al. [16] proposed an algorithm for automatically detecting flame states using video image processing, including four main calculation procedures. Firstly, a Gaussian mixture model was used to detect a moving region in frame sequences of flame images acquisition from video recording meter. The method was then applied to segment the flame motion region from the primary flame region combined with a fuzzy C-means model. This will reduce the algorithmic efficiency, until the flame image features were extracted from the region. Finally, an SVM method was utilized to distinguish between fire and non-fire regions. The experimental results showed that the proposed algorithm is superior to other flame detection algorithms,

providing higher reliability and a lower error rate. There are also examples of classification using only SVM, which will not be detailed here [17]. By creating an optimal hyperplane, an SVM classifier can well-classify fire or non-fire region in flame images captured under different circumstances. However, the results of identification are principally determined by whether the selected flame features are effective and representative. In other words, if the chosen features are poor representations of flame images, identification error could occur undoubtedly during the period of combustion diagnosis. Moreover, the SVM algorithm has difficulty in identifying some unsteady combustion situations with high similarity, making the occurrence of a specific type of misidentification more likely [13,15].

In summary, some of the above methods are suitable for identifying a flame state in pulverized coal-fired furnace or early fire, but there are still limitations in terms of prediction accuracy, computational complexity, and online-processing ability. To improve the performance of the flame detection model and develop more flame image features that are suitable for a gas-fired flame, this study developed a four-step pattern recognition method for gas-fired combustion. In the first step, the flame region in a gas-fired flame image is segmented using a logarithmic entropy multi-threshold segmentation (LEMTS) method [18]. In the second step, 12 typical features are proposed to represent gas-fired flame images, and five of these are extracted for pattern

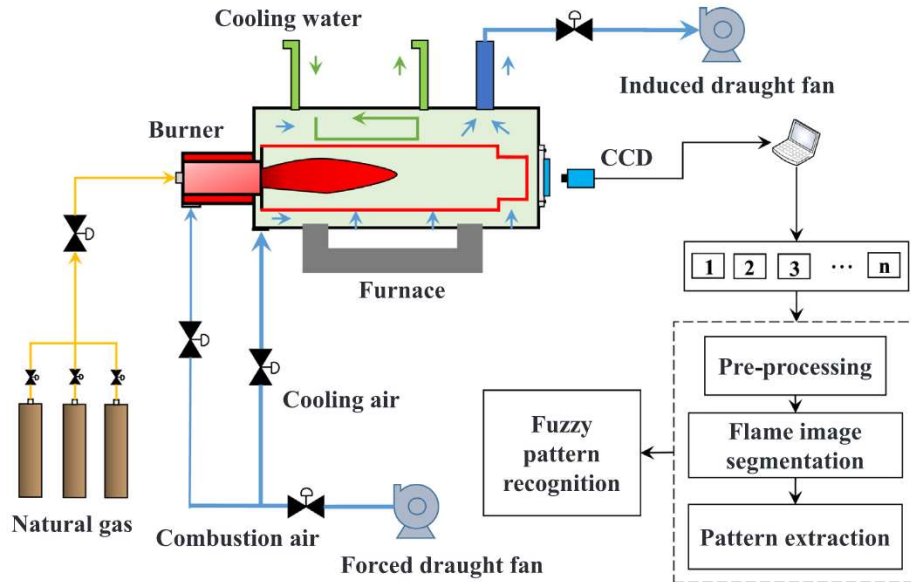


Fig. 1. Schematic diagram of the gas-fired combustion furnace and image detection system.

recognition. In the third step, different combustion situations are distinguished using a fuzzy pattern recognition (FPR) algorithm. In the final step, the recognition results are evaluated using two statistics, Q and T^2 , [19] and are compared with two other algorithms, the self-organizing map (SOM) neural network [20] and SVM [21]. The experimental results show that the method has better performance in flame segmentation, and can accurately identify the flame states under different operating conditions by adjusting the two parameters in the fuzzy model reasonably. The results of the comparison indicate that the proposed FPR method is superior to the other algorithms, and is convenient for industrial promotion and application.

2. System description and data acquisition

2.1. Gas-fired combustion experimental apparatus

For the continuous duty of a gas-fired combustion system, fire alarms must be operating and process monitoring must be conducted, for safety reasons [22,23]. To enhance the performance of intelligent monitoring of gas-fired combustion, flame image data were collected within a combustion process on a 0.3 MW gas-fired combustion experimental apparatus.

Fig. 1 shows the schematic diagram of the apparatus, mainly consisting of a gas-fired combustion system and image acquisition system. The natural gas burner was used to create non-premixed flame, and the horizontal furnace was primarily cooled by cooling water, equipped with a forced draught fan and an induced draught fan to take away heat generated by the heating from firebricks. The flow rates of fuel (natural gas), combustion air were controlled accurately by regulation valves to obtain a wide range of equivalence ratios. For capturing the flame images, a conventional CCD (Charge Coupled Device) camera (Germany eco414CVGE) was used, equipped with the industrial lens M1614-MP2. In the experiment, the camera was fixed on a tripod and oriented to the burner axis, and the camera focus was adjusted to obtain a clear flame image at a suitable viewing distance. Simultaneously, intrinsic parameters of the camera, such as the aperture, and exposure time were adjusted to suit the external environment and the needs for photographing. It was found that under unsteady operating conditions, if the aperture size of the camera was not large enough, some flame images still appeared indistinct by reducing the shutter speed (i.e., increasing the exposure time) to increase the exposure. Thus, we adjusted the aperture of the camera to a maximum of f/1.0 based on the low-load working conditions, to better capture the flame images for abnormal combustion. As a result, flame images under high-load conditions were approaching saturation or even over-exposure, causing some physical information of the flame to be lost. Accordingly, the exposure time was calibrated to 3000 μ s based on a comparative observation, so that the

flame structure for unsteady combustion was distinctly clear, on the premise that abnormal flame images could also be noticeably captured. It is worth mentioning that this study does not have high requirements for optical precision and only requires for distinguishable flame structure in two-dimensional (2D) image, extracting some non-physical features of a flame for further pattern recognition.

By adjusting the mass-flow rate of natural gas and combustion air accurately, different equivalence ratios could be determined to simulate combustion operating conditions, so that the flame image of gas-fired combustion in various combustion processes (ignition, extinguishing, etc.) could be obtained. After that, the image data obtained by CCD were processed using filtering and grayscale operators, and the post-processed flame images were segmented by a LEMTS method. Then, characteristic parameters of flame images were extracted using the proposed feature models for use in the next step, entitled “FPR”. Thus, a gas-fired combustion monitoring system based on image processing technology was designed.

2.2. Flame image data acquisition

Flame images captured from different angles induce different image features, especially in regards to geometric parameters, which have restrictions on the choices of flame features in the early stage of pattern recognition. In that regard, scholars continue to take flame images from different camera angles. Duo Sun et al. [4] placed an observation port at the root region of a heavy-oil-fired flame and used a digital imaging and spectral analysis system to detect the flame, to extract parameters such as ignition points, luminous region, flame brightness, non-uniformity, and oscillation frequency. Y. Yan et al. [24] also observed a pulverized coal flame at the root of the flame, and apart from the parameters discussed above, spreading-angle along the direction of flame height was extracted. In addition, Yingping Huang et al. used a CCD to observe from the side of a flame [25]; and Hao Zhou et al. [17] installed a flame monitoring system at the outlet of a burner to obtain coal-fired flame images and light intensity signals. These various measurement methods have been used not only extract and establish reliable flame image features, but also to establish feasible evaluation criteria of flame states.

In our experiment, the lens of CCD was oriented toward the axis of the gas-fired burner, different from the conventional acquisition methods of flame images regarding observation direction. This method sacrificed some flame information along the depth of the horizontal furnace, including flame height, lateral area, and other features. In other words, it can find more flame features at a particular camera angle, laying a foundation for multi-angle coordinated monitoring of gas-fired combustion. This study investigated the steady and unsteady combustion processes of gas-fired flames under different fuel loads (60–100%, where 100% represents a mass-flow rate of natural gas of

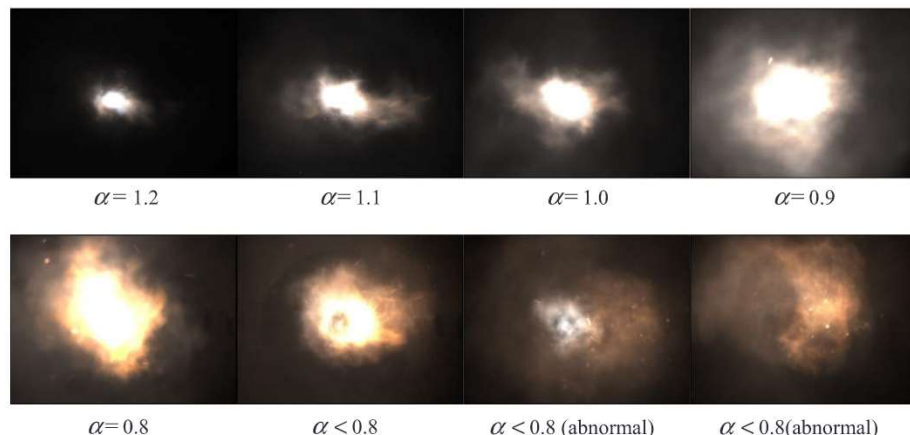


Fig. 2. Gas-fired flame images for different equivalence ratios (100% load).

$30 \text{ m}^3 \text{ N/h}$) and equivalence ratios (0.8–1.2, where 1.0 represents complete combustion, and under 100% load, a mass-flow rate of air is $289 \text{ m}^3 \text{ N/h}$).

Fig. 2 shows a series of flame images (RGB image, 492×656 pixels, exposure time $3000 \mu\text{s}$) taken at different equivalence ratios under a full gas-fired load. α represents the equivalence ratio, which is defined as a ratio of the actual fuel-to-air ratio to the stoichiometric fuel-to-air ratio. These images were selected to observe any extraordinary features of gas-fired flame under specific camera parameters. Some flame images appeared overexposed, but it did not have significant effect on the observation of flame structure. In fact, differences were found between various regions in the same flame image, mainly in regards to the saturation and brightness characteristics. Owing to the large exposure, flame images under unsteady combustion conditions were captured distinctly, helping us to mine the potential features of these abnormal flames. As can be seen, under steady operating conditions ($0.8 \leq \alpha \leq 1.2$), the flame images only varied in the size of flame region, and the geometric and luminous parameters of the flame did not change much. As the equivalence ratio decreased to 0.8 (a fuel-lean condition), the flame stability of gas-fired combustion gradually decreased and it was difficult for a flame to maintain the steady combustion. It was evident that at a full gas-fired load, when α was close to or less than 0.8, a flare or flash appeared in the flame image, and the color of the corresponding combustion region began to darken, saturation decreased, and the overall flame rapidly blew out. This indicated that the gas-fired combustion had started to become abnormal and it is necessary to adjust the fuel air ratio to ensure the steady and continuous operation of the burner.

3. Flame detection model of gas-fired combustion based on fuzzy pattern recognition

As compared to conventional flame detection techniques using inflexible sensors, a large amount of information can be extracted from a flame image, providing a more practical combustion diagnostic method [26–29]. The flame image contains not only the brightness information of the flame, but also texture information, flicker frequency, and other characteristics [2,4,6,26]. Often, it is essential for researchers to extract more representative features from flame images for the assessment of the flame stability in combustion processes. Many characteristic parameters have been proposed for pattern recognition using flame images, and these parameters can better distinguish between states of flame stability or non-stability. This research is aimed at finding several novel and effective parameters for evaluating the stability of a gaseous flame, as well as a new method for identifying gas-fired flames under diverse combustion situations.

3.1. Pre-processing and gas-fired flame image segmentation

In the process of analyzing a gas-fired flame image, the reliability and accuracy of the image data play an important role in extracting all of the flame features. However, owing to environmental impact and losses of signal intensity in data transmission, there can be many mechanical noises in the directly-obtained flame image data [30]. In this study, a median filtering method was used to reduce nonlinear noise in the image data, and the filtered flame images were converted to grayscale images before segmentation [31]. Then, a segmentation method called LEMTS was used to segment the candidate flame regions.

For a gaseous flame, the abnormality of a flame state can be easily reflected by different image features under a particular operating condition, such as luminous and geometric parameters. In order to obtain flame images of abnormal combustion, we increased the exposure of the camera to make these flames visible under a low gas-fired load, but this caused the gaseous substance around the flame to emit light in the flame image, making it difficult to segment the flame region. It is known that the combustion process of natural gas-fired flame (mainly

methane) will release large quantities of combustible or non-combustible products, especially H_2O (in the form of water vapour) and CO_2 . Generally, a complete combustion of a gas-fired flame means a high level of saturation and brightness in the center of a flame image, and those regions of high luminous intensity are likely to be the flame region. The slightly darker region around the flame is probably formed by the combustion products at the location of reaction fronts releasing significant amounts of radiation. Besides H_2O and CO_2 , there may be many other substances in this region, such as CO , NO_x , soot, and some excited radicals in the visible band (including the possibly unburned air or natural gas). These combustion products will emit light physically or non-physically under particular combustion condition, making a difference to the performance of flame segmentation. Moreover, they are easy to diffuse upward along the internal surface of the furnace wall, continuously absorbing and releasing heat from the flame and fire-bricks. Reflected in the 2D image, the gas-fired flame region is tightly surrounded by these substances and the luminous intensity of this region is similar to that of the darker region. Therefore, the flame region cannot be well-extracted using a binary image segmentation method. Furthermore, these flame images were taken at large exposure, and there could be some optical distortion on the luminous intensity of the flame. It was entirely possible that the darker area of each image was caused by overexposure, whereas this did not excessively degrade the performance of the segmentation method used. Although some details of the flame were obscured by possible noise, it could be found that the flame body was retained and the background of the burner was cleanly filtered. The results proved that such camera parameters were better for capturing abnormal flame and provided a robust capability of flame segmentation under a wide range of equivalence ratios.

The LEMTS method focuses on a fine distinction of optical properties of different regions in a flame image, and improve the classification capacity for the flame region [18]. For example, the flame region and the supposed region of combustion products in a 2D flame image are mixed due to the similar brightness, making it difficult to segment the flame region. By seeking the equilibrium distribution of log-entropy of different regions, the LEMTS method can divide the gray-scaled image of a flame into multiple regions accurately and effectively. It was found that it was more appropriate to choose two thresholds to divide the flame image into three regions. In these three regions, the brightest region in a flame image will be the flame region. It is considered that the darker region around the flame may be a region where a large amount of combustion products accumulates, and it is named as a radiation region of the combustion products. In addition, the darkest region is defined as the background region. In fact, different gaseous substances can be distinguished by measuring the wavelength of the infrared spectrum, but this study focuses only on the extraction of the flame region by using image-processing method based on the LEMTS. The following will briefly introduce the LEMTS method [18].

The captured flame image is the 2D distribution of luminous intensity of the 3D flame onto the CCD imaging plane. Assume that the size of a flame image is $M \times N$, and that each pixel point (m,n) in the flame image is composed of three RGB colors. When the RGB image is converted to gray-scaled image, $G(m,n)$ represents the gray-level intensity $0, 1, \dots, L-1$ of each point (greyscale:256-bit). Suppose that t is a threshold for distinguishing between different gray levels, and that h_i represents a frequency with a gray level i (i from 1 to t). Then, the log-entropy function H is calculated as

$$H = - \sum_{i=0}^t h_i P_i \ln P_i \quad (1)$$

The value of H represents the gray-level uniformity of pixels of a region. Here, P_i represents a probability value regarding the gray level i in the gas-fired flame image, and it can be defined as

$$P_i = i \left/ \sum_{j=0}^t h_j \right. \quad (2)$$

If n thresholds t_i (i from 1 to $L-1$) are needed to divide the image into $n + 1$ regions, the log-entropy function of multiple thresholds can be calculated as

$$H(t_1, t_2, \dots, t_n) = - \sum_{i=0}^{t_1} h_i P_i \ln P_i - \sum_{i=t_1+1}^{t_2} h_i P_i \ln P_i - \dots - \sum_{i=t_{n-1}+1}^{L-1} h_i P_i \ln P_i \quad (3)$$

After that, expression (4) is applied to represent the optimal threshold vector T^* .

$$T^* = \arg \max_{0 \leq i \leq L-1} \{H(t_1, t_2, \dots, t_n)\} \quad (4)$$

To find the optimal thresholds (dual-threshold segmentation was adopted) for segmenting the flame image, the particle swarm optimization algorithm (PSO) was used in this study. In detail, the fitness of a particle in PSO algorithm is represented by its fitness function, entitled the “log-entropy function”, which has been defined above. Suppose that each particle has a position $x_i = (x_{i1}, x_{i2}, \dots, x_{in})$, and that x_i represents the solution of the segmentation issue. Then, the speed update formula and the position update formula can be defined as in Eqs. (5) and (6). Additional details can be found in the literature [32].

$$V^{k+1} = wV^k + c_1 r_1 (P_{id}^k - X^k) + c_2 r_2 (P_{gd}^k - X^k) \quad (5)$$

$$X^{k+1} = X^k + V^{k+1} \quad (6)$$

In the above, V^k represents the current speed of the particle, X^k represents the current position of the particle, P_{id} is the individual optimal position, P_{gd} is the group optimal position, r_1 and r_2 are random numbers between 0 and 1, and w is the inertial factor. The termination condition of the PSO algorithm is as follows: (1) a specified number of iterations is reached; or (2) the difference between the positions satisfies the minimum limit.

Fig. 3 shows the results of segmentation on flame images using the LEMTS method. a (1) is a flame image captured under a steady

combustion situation, b (1) is an image of the flame captured at the transition period, and c (1) depicts an unstable flame. As can be seen, for an unstable gas-fired flame, the corresponding flame image exhibited abnormal characteristics. For instance, a hole with low luminous intensity appeared in the flame region (in Fig. 3 b (1)), or the flame shape became uneven, and the unbroken appearance was no longer presented due to the gradual deterioration of combustion. This phenomenon is critical for finding useful characteristic parameters of flame image. Meanwhile, as the gas-fired combustion began to become abnormal, parameters such as the flame area and flame brightness could be sharply changed, as can be seen from the segmented images a (4), b (4), and c (4). A detailed description can be found in the section of pattern extraction below. In addition to these significant changes in the appearance of a flame, it can also be found that the processed flame images are well-separated, and the three parts can be extracted effectively, whether in normal or abnormal combustion situations. It is apparent that the white regions in a (4), b (4), and c (4) are flame regions for complete combustion, and the darker regions around the flame may be the radiation region of the combustion products. The two regions are segmented separately and strictly to better observe the abnormal flame, or some details of incomplete combustion cannot be found. As already noted, the black regions in these images are background regions.

3.2. Pattern extraction

Pattern recognition method based on flame images are primarily concerned with luminous or geometric features in combustion of solid and liquid fuels, such as pulverized coal flames or oil-fired flames. For example, Duo Sun et al. proposed a method for monitoring the state of a 9 MW heavy oil-fired combustion process based on feature extraction and KPCA, and extracted the flame area, brightness, non-uniformity, and oscillation frequency, among other features. Then, they proposed the Q and T^2 statistics for diagnosing an unsteady combustion of a flame [18,33]. John Smart et al. used image processing technology to study the oxy-coal combustion flame, and measured the flame temperature and oscillation frequency to characterize the flame features [34]. A. GonZalez-Cencerrado et al. [27] processed flame images in a 500 kW

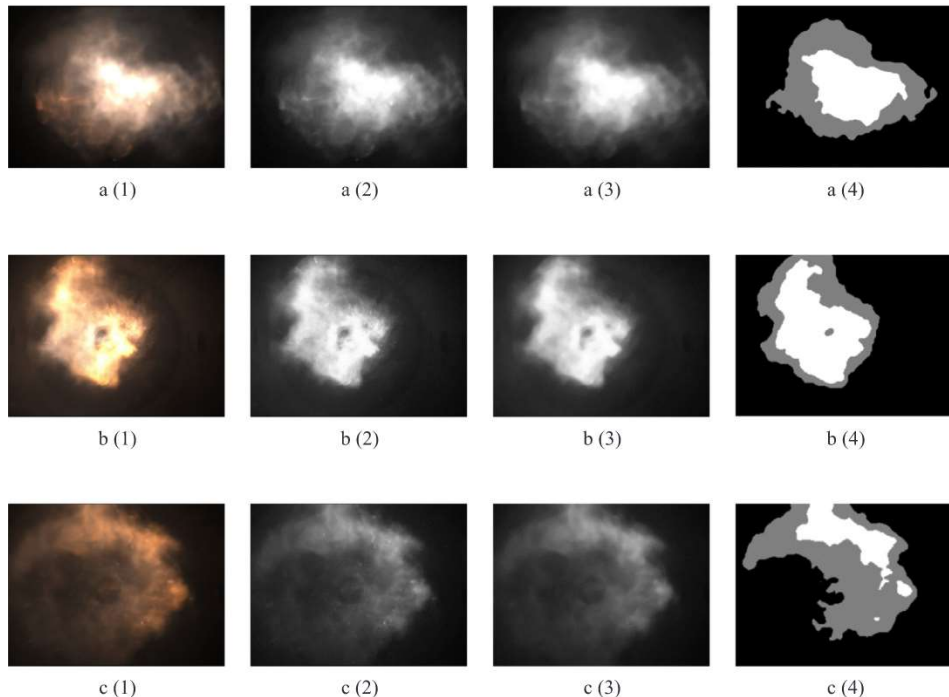


Fig. 3. Normal and abnormal gas-fired flame images and segmentation results. a (Normal combustion); b (Transition state); c (Abnormal combustion) (1) Original image (2) Gray image (3) The filtered image (4) The segmented image by log-entropy dual-threshold method.

eddy-stabilized semi-industrial burner, and extracted luminous parameters (such as brightness, brightness volatility, and volatility symmetry) and spectral parameters (power spectrum, pixel density, and flicker frequency). Duo Sun et al. [4] combined optical sensing, image processing, spectral analysis, and other technologies to detect the light intensity of a flame in two beams (relevant flame image features were mentioned above). Wang Jiesheng et al. [9] used a gray symbiotic matrix to extract 13 texture features from coal-fired flame images. Y. Yan et al. combined optical sensing, digital image processing, and other technologies to continuously visualize a flame in a pulverized coal furnace, and used the imaging system to extract geometric and luminescence parameters of the flame, such as the luminous area, centroid, ignition point, diffusion angle, brightness, uniformity, and standard deviation of each characteristic parameter [24]. K. Sujatha et al. [12] extracted a flame area, brightness, orientation, and other characteristics from quality monitoring of combustion processes in a power generation plant. Yingping Huang et al. [25] used a neutral filter, monochrome CCD, and frame-grabber to extract flame flicker frequency through power spectrum analysis.

The above scholars have effectively monitored the combustion situation of a flame in terms of flame geometric parameters, luminous parameters, frequency parameters, etc. However, most of the proposed flame features do not satisfy the requirements for monitoring a gaseous flame, especially when the CCD lens was directly aligned with the burner nozzle. Therefore, it is necessary to create novel and independent features to adapt to a special measurement mode for gas-fired combustion, and to evaluate the gas-fired flame stability quantitatively. In addition, there is also a need for a new method of pattern recognition based on these features, to thereby improve the prediction accuracy of abnormal combustion of a gas-fired flame. This study presents several new image features for a gas-fired flame, and the following section provides a brief introduction to these features.

Total flame area: The total area of the flame region can be used to help visualize the dynamic combustion process of a gas-fired flame intuitively and it is calculated based on the number of pixels in the flame region.

$$S_f = \sum_{m \in f} \sum_{n \in f} g(m, n) \quad (7)$$

$$g(m, n) = \begin{cases} 1 & \text{if } G(m, n) > \delta \\ 0, & \text{other} \end{cases} \quad (8)$$

Here, m, n respectively represent coordinates in the flame image, $G(m, n)$ represents the gray value of the pixel point (m, n) , and δ is one of the optimum thresholds in vector T^* for distinguishing a flame region from an expected radiation region of combustion products. As the fast-changing threshold is solved by the PSO algorithm described above, the total flame area is constantly changing during the combustion process.

Area ratio: This study used a multi-body segmentation method to extract the main bodies of the flame region. Fig. 4 is an example of the method under an abnormal combustion situation. The core portion of the flame region is defined as the largest body of the flame (LBF, blue part in Fig. 4(c)), whereas the second part segmented in the flame region is defined as the derived body of the flame (DBF, red part in

Fig. 4(c)). According to these definitions, the area ratio of the flame is described as the ratio of the area of LBF to the area of DBF. This parameter can be used to observe a flare or flash in the flame image and it is important for monitoring the abnormal combustion of a gas-fired flame. The area of DBF may be extremely small or even 0, making the flame image a large sparse matrix, which is inconvenient for image processing. Therefore, in this study, a pre-given threshold was used to impose restriction on the area of DBF, i.e., when the area exceeds 5000 pixels, it is included in the calculation, otherwise it is defined as 0. Obviously, the threshold here is a hyper-parameter, and it has been found that 5000 should be more suitable for diagnosing an abnormal flame.

Rectangular fullness: The rectangular fullness of the flame is determined by the proportion of the flame area filling a bounding box in the image. It is defined as the ratio of the area of LBF to the area of the bounding box of the flame, and it can be represented by using the ratio of the pixel numbers in these two regions. This feature has similar effects as that of the circularity of the flame (discussed later), but experimental results show that the effect of the rectangular fullness on reflecting the flame combustion stability is much better than that of the circularity. Fig. 5 is an example of extracting a rectangular fullness of the flame; the area of the bounding box is calculated by the largest red rectangle algorithm [35].

Connectivity: The connectivity of the flame can evaluate the shape of the flame region and indicates whether and to what extent the segmented flame region becomes a single and non-porous body. The flame image of gas-fired combustion show that when the flame stability begins to decrease, significant holes may appear in the image of the 2D body of the flame. Moreover, under an unsteady combustion situation, the flame will spread around the wall of the furnace, decreasing in brightness and saturation, and will no longer maintain the original shape. The connectivity of the flame is a good description of these changes in flame stability, and is defined as in Eq. (9).

$$\Omega = \left(\frac{\sum_{i=1}^m \sum_{j=1}^n g(i, j)x^{(i)}}{x_{\max}^{(i)} - x_{\min}^{(i)}} \right) / m \quad (9)$$

Here, m represents the maximum number of rows of the flame region, n represents the maximum number of columns of the flame region, x represents the horizontal coordinate of the whole image, x_{\max} represents the maximum horizontal coordinate of the flame region, and x_{\min} represents the minimum horizontal coordinate of the flame region. In this study, the resolution of the gas-fired flame image was 492(H) × 656(V) pixels, and each coordinate value did not exceed the limit value.

In addition to the features discussed above, some of the flame image features have been proposed by many predecessors were also used by this study. The following part is a brief introduction to these features, and the relevant content can be found in [2, 18, 27].

Circularity: The circularity of the flame can be used to measure the uniformity of the 2D distribution of the flame. Assuming that there is an equivalent circle with the same flame area S_f , the circularity is defined as the ratio of the perimeter of the circle $C_{eq} = 2\sqrt{\pi S_f}$ to the perimeter

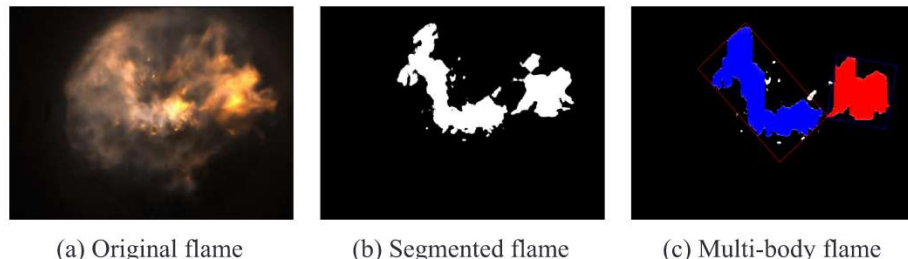


Fig. 4. Example of multi-body extraction from gas-fired flame image. (a) Original flame (b) Segmented flame (c) Multi-body flame.

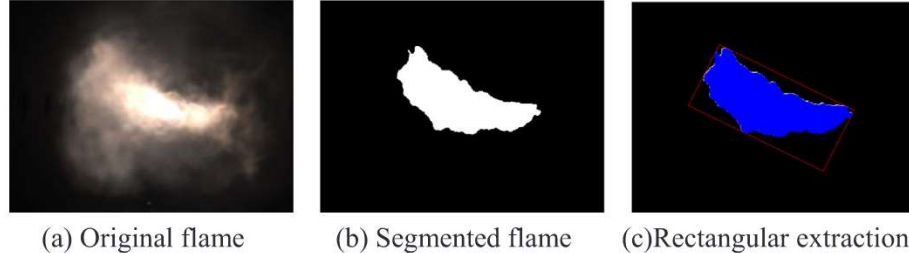


Fig. 5. Example of the rectangular fullness extraction from gas-fired flame image. (a) Original flame (b) Segmented flame (c) Rectangular extraction.

of the flame region C_f . This flame feature is calculated based on the LBF.

$$\Phi = C_{eq}/C_f \quad (10)$$

Mean value of grayscale: The mean value of grayscale of the flame represents the average gray-level intensity of the flame region.

$$G_A = \sum_{(i,j) \in S_f} g(i, j)/N_f \quad (11)$$

Standard deviation of gray-level intensity: The standard deviation of the gray-level intensity of the flame image indicates the uniformity of the distribution of grayscale in the gray-scaled flame image.

$$\sigma = \sqrt{\sum_{(i,j) \in S_f} (g(i, j) - G_A)^2/N_f} \quad (12)$$

Gray entropy: The gray entropy of the flame image indicates the non-uniformity of the distribution of the flame brightness, and plays a similar role to the standard deviation of gray-level intensity.

$$E = - \sum_{i=0}^n h_i P_i \ln P_i, P_i = i / \sum_{j=0}^n h_j \quad (13)$$

Mean value of B channel and R channel: The mean value of B channel or R channel respectively represents the average intensity of blue or red channel of the RGB flame image (It was found that the change of R channel was not significant for gas-fired flame).

Geometric center and luminous centroid: The geometric center represents the central position of the flame region, whereas the luminous centroid indicates the central position of the brightness of the flame region.

$$(G_x, G_y) = \left(\frac{\sum_{(x,y) \in S_f} x}{\sum_{(x,y) \in S_f} 1}, \frac{\sum_{(x,y) \in S_f} y}{\sum_{(x,y) \in S_f} 1} \right) \quad (14)$$

$$(M_x, M_y) = \left(\frac{\sum_{(x,y) \in S_f} f(x, y)x}{\sum_{(x,y) \in S_f} f(x, y)}, \frac{\sum_{(x,y) \in S_f} f(x, y)y}{\sum_{(x,y) \in S_f} f(x, y)} \right) \quad (15)$$

Fig. 6 shows a typical combustion process of approximately one minute, where various characteristic parameters of a flame change as the equivalence ratio decreases. The ignition and steady combustion of gas-fired flame last for a total of 40 s and then the combustion situation starts to become unsteady for about 14 s. The changing trend of each flame image feature shows some evident changes, including those of the total flame area, area ratio, connectivity, rectangular fullness, standard deviation of the gray-level intensity, and mean value of B channel.

Fig. 6(a) illustrates the variation trend of the total flame area as the equivalence ratio α decreases. It can be seen that the total flame area climbs to a peak, and then decreases sharply at around frame 150 until it fails to 0, accompanied by a gas-fired flame converted from normal to abnormal combustion. The continuous change of this characteristic shows the dynamic response of the gas-fired flame to the equivalence ratio intuitively. From **Fig. 6(b)**, it can be found that when the flame is stable, the area ratio of the flame is almost close to 0, but when it

becomes unstable, this parameter will immediately oscillate between 0 and 1, especially when α is smaller than 0.8 (a fuel-lean condition). Therefore, the area ratio of the flame is a well-behaved parameter for monitoring on flame states, and can be used to diagnose the abnormal combustion by itself. However, further study is still required on how to use the area ratio of the flame more reasonably. At the same time, the signal intensities of connectivity, rectangular fullness, standard deviation of the gray-level intensity, and mean value of B channel will show a step response during the transition from normal to abnormal combustion regime. For an unsteady combustion process, the variance of each characteristic parameter is larger than that in a steady combustion process, which is also an obvious sign of abnormal flame state. In addition, some of features (such as the circularity and the mean value of grayscale of the flame) do not show remarkable differences between variable combustion conditions. Other characteristic parameters, such as the log-entropy and several centroids of the flame, have little impact on the pattern recognition herein. Thus, the trends of these features are not shown.

3.3. Fuzzy pattern recognition

After extracting image features of the gas-fired flame described above, the FPR model was used to distinguish between an abnormal flame state and a normal flame state. FPR is a fuzzy-based classification method using fuzzy rules, and by operators of fuzzification and defuzzification, it can solve problems with fuzzy properties [36–38].

In this study, a two-class classification model was implemented to give the prediction label of an unknown flame image and the flame stability could be measured based on the decision-making method of the fuzzy classifier. The fuzzy operation was employed using a custom S-function to calculate the membership grade corresponding to the known pattern of the gas-fired flame image. Eq. (16) is the proposed model of membership function (shown in **Fig. 7**), as a mapping rule to provide a fuzzy representation for the selected characteristic parameters of the gas-fired flame.

$$f(x_i) = \begin{cases} 0 & 0 \leq x_i < C_1 \text{ or } x_i = -1 \\ \frac{1}{1 + \left| \frac{x_i - C_2}{x_i - C_1} \right| e^{-(x_i - a)/b}} & C_1 \leq x_i < C_2 \text{ and } i = 1 \\ 1 - \frac{1}{1 + \left| \frac{x_i - C_2}{x_i - C_1} \right| e^{-(x_i - a)/b}} & C_1 \leq x_i < C_2 \text{ and } i = 2, \dots, 5 \\ 1 & x_i \geq C_2 \end{cases} \quad (16)$$

Here, x_i represents the value of a characteristic parameter labeled i (from 1 to 5); a , b , C_1 , and C_2 are defined as in Eqs. (17), (18), and (19); the expression of $x_i = -1$ (for all i) represents that the combustion process has stopped, leaving only background region in the flame image; additional detail regarding the selection of coefficients can be found in the literature [39].

$$a = \eta \left(\sum_{j=1}^{n_1} x_{ij}^{(1)} / n_1 + \sum_{j=1}^{n_2} x_{ij}^{(2)} / n_2 \right) \quad (17)$$

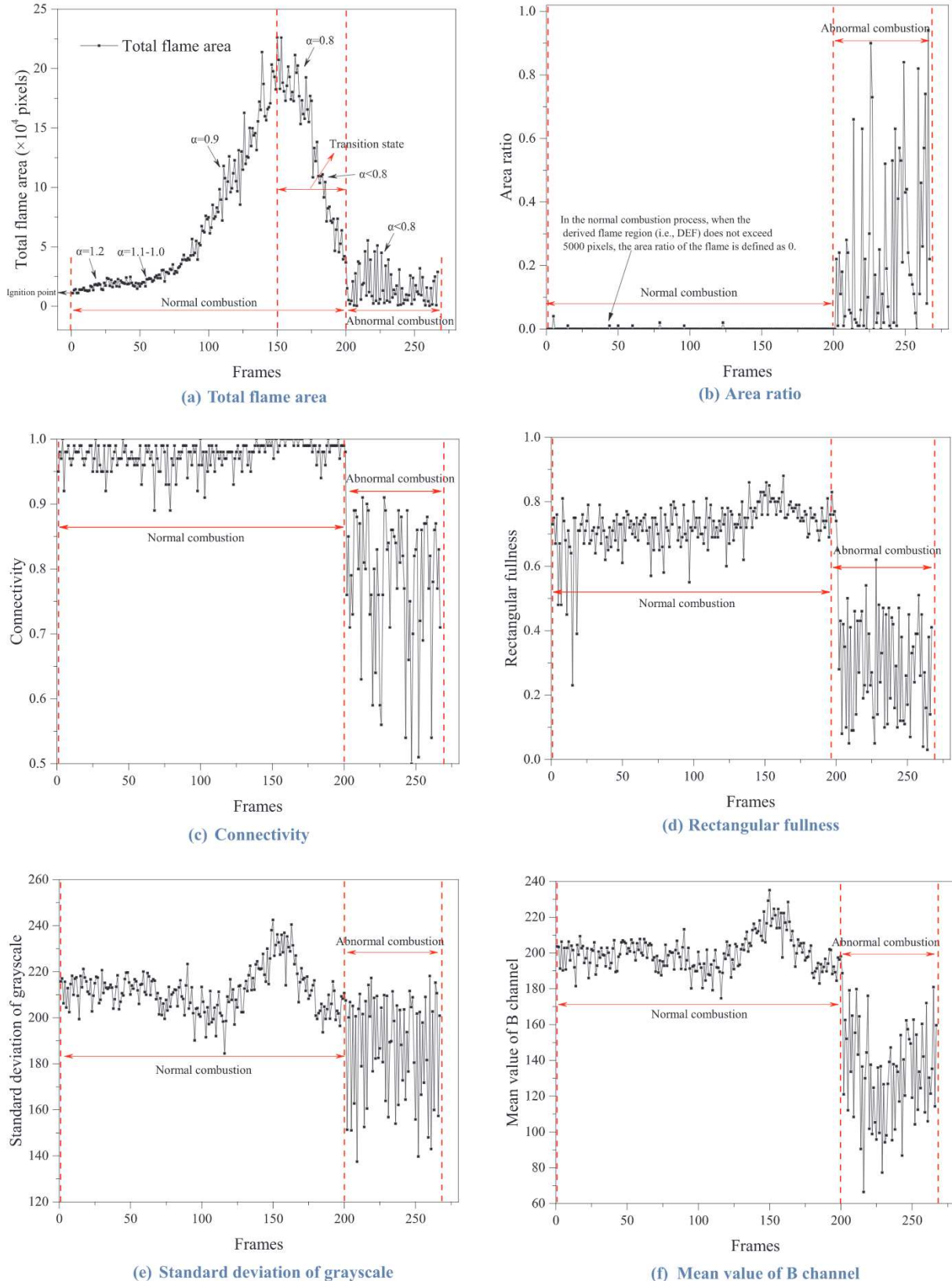


Fig. 6. Several characteristic trends of gas-fired flame under the decreasing equivalence ratio (5 frames/s). (a) Total flame area (b) Area ratio (c) Connectivity (d) Rectangular fullness (e) Standard deviation of grayscale (f) Mean value of B channel.

$$b = \max \left\{ \sqrt{\sum_{j=1}^{n_1} (x_{ij}^{(1)} - \bar{x}^{(1)})^2 / n_1}, \sqrt{\sum_{j=1}^{n_2} (x_{ij}^{(2)} - \bar{x}^{(2)})^2 / n_2} \right\} \quad (18)$$

$$C_2 = \max\{x_{ij}\}, C_1 = kC_2, j = 1, \dots, n_1 + n_2 \quad (19)$$

In the above, η and k are hyper-parameters between 0 and 1, which are pre-defined in advance (initially, $\eta = 0.5$, and $k = 0.3$). The index

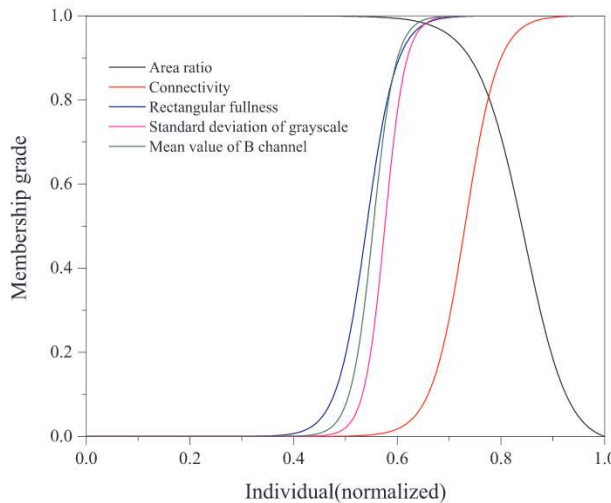


Fig. 7. Membership function of the selected five gas-fired flame image features.

(1) in $x_{ij}^{(1)}$ (j from 1 to n_1) represents a steady combustion situation, whereas (2) in $x_{ij}^{(2)}$ (j from 1 to n_2) represents an unsteady combustion situation. n_1 and n_2 respectively represents the maximum number of frames obtained from both of the conditions. Each group of coefficients (a , b , C_1 , and C_2) calculated for each characteristic parameter was represented by a vector with a length of four. By time series analysis of each characteristic parameter, five representative parameters had been selected as engineering features for the training of FPR model. These parameters were labeled from 1 to 5 in this order: area ratio, connectivity, rectangular fullness, standard deviation of grayscale, and mean value of B channel. It was demonstrated that sequential data of these parameters exhibit significant differences in mean value and variance during the transition to unsteady combustion, thereby aiding in identification.

The training and the testing data of flame features need to be normalized before the calculation of membership grade, to scale the data matrix to the [0,1] range (applied a max-min method). Meanwhile, a max-min distance function was used to calculate the relative approach degree between the flame characteristics to be identified and the known flame characteristics [36,37]. In terms of classification of flame states, the feature vector of a stable gas-fired flame was defined as a known vector [1, 1, 1, 1, 1]. After calculating the relative approach degree between the unknown vector and [1, 1, 1, 1, 1], a static threshold was provided to determine if the flame was stable, or if the flame had been extinguished (after testing, it was found that the threshold was suitable between 0.4 and 0.5). The max-min distance function based on fuzzy operation can be defined as in Eq. (20).

$$\sigma(A, B) = \frac{\sum_{i=1}^n (A(x_i) \wedge B(x_i))}{\sum_{i=1}^n (A(x_i) \vee B(x_i))} \quad (20)$$

$\sigma(A, B)$ represents the relative approach degree between two flame feature vectors (A and B) extracted from images and the x_i (i from 1 to 5) here has been standardized by the operation of fuzzification; \wedge indicates minimizing, whereas \vee indicates maximizing. This distance function can be used as a fuzzy-based classifier to determine a flame state by making a judgment at a given threshold. To get the solution of formula (20), input vectors of both A and B must be consisted of the value of each characteristic parameter after fuzzification (these values are between 0 and 1 and include 0 and 1). Additional detailed information can be found in the literature [36].

Table 1
Training and testing image data sets of gas-fired flame (5 frame/s).

Objective	The combustion process	Image frames
Training 1	Normal	3600
Training 2	Abnormal	50
Testing case 1	Normal	900
Testing case 2	Abnormal	66
Testing case 3	Ignition	1780
Testing case 4	Flameout	43

4. Case studies: Fuzzy pattern recognition model

In the training process of pattern recognition model, the batch size of training data set plays a crucial role in the accuracy of identification, especially for models that need to be optimized by gradient descent algorithm. Furthermore, a good training data set must ensure that all the features are covered by a sufficient number of samples, which should receive more attention in feature engineering. In this study, nine sets of normal frames (400 frames per data set) and one set of abnormal frames (50 frames) were used to obtain the coefficients of fuzzy model. Some continuous combustion processes of gas-fired flame were utilized as the testing data sets, such as the ignition process (1780 frames) and the flameout process (43 frames).

A few flame images were captured under abnormal combustion processes due to the danger of deflagration, which would reduce the accuracy of identification results, because it failed to obtain as many abnormal flame images as possible (in Table 1). For this reason, data augmentation can be used to increase the number of training data when the model is faced with underfitting problem.

In this study, gradient calculation or error propagation algorithm were not involved in the training process, so it was not a necessity for a reasonable ratio of training/testing set. In fact, the coefficients of the fuzzy model were easily calculated by mean value and variance of each batch of training samples, so no further enrichment of the original image data was implemented. Table 2 shows the mean value of each feature after fuzzy mapping under different operating conditions. In a steady combustion situation, the mean value of membership degree of each feature is basically above 0.9, while it will drop to nearly 0 under an abnormal combustion process, such as the flameout process. This indicates that the study successfully widened the distinction of flame characteristics under different combustion conditions, advantaging in pattern recognition. It is worth noting that the ignition process shows the property of chaos and in the captured frame sequence, it is uncertain for the proportion of the number of flame images under variable combustion situations, resulting in a slight decrease in the averaged membership grade.

Table 2

Mean value of membership grade under different gas-fired combustion conditions. (a: Area ratio, b: Connectivity, c: Rectangular fullness, d: Standard deviation of grayscale, e: Mean value of B channel).

Gas-fired Load (100%: 30 m ³ N/h)	Equivalence ratio	a	b	c	d	e
60%	0.8	1.00	0.91	0.80	0.63	0.87
	1.0	1.00	0.92	0.89	0.90	0.91
	1.2	0.99	0.95	0.89	0.91	0.89
80%	0.8	1.00	0.95	0.91	0.96	0.93
	1.0	1.00	0.97	0.94	0.96	0.97
	1.2	1.00	0.97	0.85	0.94	0.91
100%	0.8	1.00	0.96	0.92	0.88	0.91
	1.0	1.00	0.96	0.90	0.97	0.96
	1.2	1.00	0.97	0.86	0.95	0.92
Abnormal combustion process		0.74	0.34	0.11	0.06	0.18
The ignition process		0.99	0.82	0.66	0.55	0.75
The flameout process		0.14	0.11	0.06	0.03	0.05

5. Results assessment

To verify the reasonability and availability of the model, two statistical methods commonly used in fault diagnosis were introduced to evaluate the results of FPR. Simultaneously, the results were compared with those of other popular recognition algorithms. Then, the two empirical parameters in FPR model were quantitatively studied.

PCA-based fault detection is a well-developed method in the fields of flame detection and digital image processing [14,40,41]. For instance, Duo Sun et al. [33] proposed a KPCA method that used Q and T^2 statistics to facilitate process monitoring and fault diagnosis, achieving a good performance for flame detection. Both of the statistics based on PCA/KPCA were used to diagnose a flame state represented by a feature vector and the assessment results of them were compared with those of FPR. Notably, the same training data were utilized here to train the PCA/KPCA model. The mechanism of PCA-based method is not described in detail here, but the corresponding statistical expression is briefly provided. Further details can be found in the literature [33].

The Q statistic is known as a squared prediction error, and it can evaluate the goodness-of-fit of a new feature vector to the residual space of the PCA model. In this study, the residual vector (obtained by PCA) of the testing data was used for diagnosis. The Q statistic is defined as in Eq. (21).

$$Q = \|\hat{x}\|^2 \leq \delta^2 \quad (21)$$

Here, \hat{x} represents the residual vector to the PCA model, and δ^2 is the confidence limit of Q statistic. The T^2 statistic can evaluate the variation of a new feature vector within the principal component space of the PCA model and it can be defined as:

$$T^2 = x^T P \Lambda^{-1} P^T x \leq \chi^2 \quad (22)$$

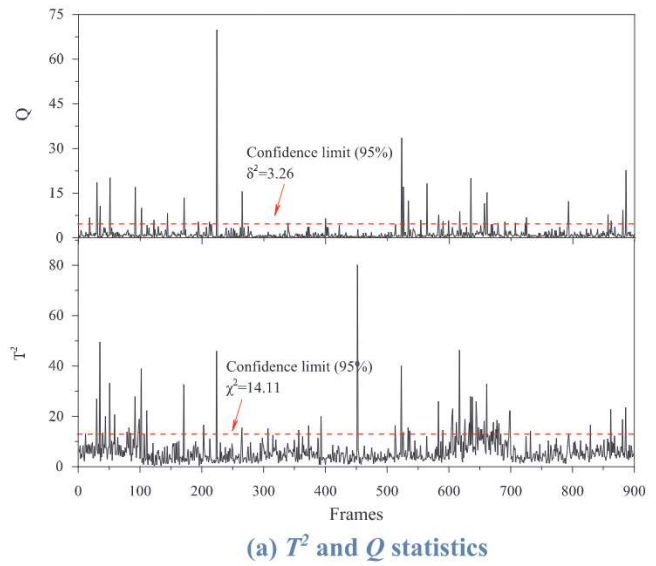
In the above, Λ^{-1} is a diagonal matrix (composed of the inverse of eigenvalues of the adopted kernel matrix), x is a new feature vector to be tested, P is the principal component matrix of training data (calculated by KPCA), and χ^2 is the confidence limit of T^2 statistic. Additional details can be found in the literature [33].

In some cases, it may be more convenient to evaluate different combustion states using a single value. Yue [19] proposed a method combining both of the above-described statistics; this study also used it as a composite indicator to conduct stability assessment on flame states, and φ statistic (The confidence limit of φ is ψ^2) is defined as in Eq. (23).

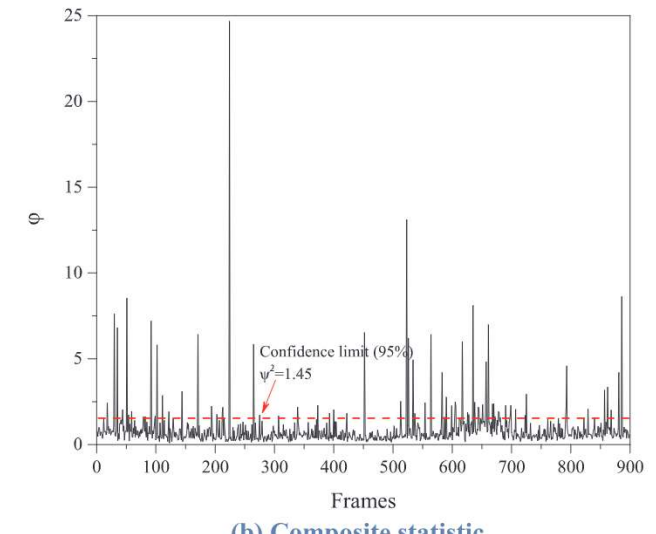
$$\varphi = \frac{Q}{\delta^2} + \frac{T^2}{\chi^2} = x^T \Phi x \quad (23)$$

$$\Phi = \frac{P \Lambda^{-1} P^T}{\chi^2} + \frac{I - PP^T}{\delta^2} \quad (24)$$

The identification results of flame states under testing operation cases are shown in Table 3. It can be seen that, as compared with Q and



(a) T^2 and Q statistics



(b) Composite statistic

Fig. 8. 900 frames of normal gas-fired combustion condition. (a) T^2 and Q statistics, (b) Composite statistic.

T^2 statistics, the FPR model has a higher prediction accuracy (100%) for normal combustion processes and a lower prediction accuracy ($\geq 90\%$) for abnormal combustion processes. For abnormal processes (including

Table 3
Identification results under different combustion conditions.

Gas-fired load (100%: 30 m ³ /N/h)	Equivalence ratio	Prediction accuracy			φ	Standard deviation
		FPR	Q	T^2		
Normal combustion	60%	0.8	100%	93%	91%	85%
		1	100%	92%	97%	7%
		1.2	100%	89%	97%	7%
	80%	0.8	100%	96%	96%	94%
		1	100%	97%	99%	98%
		1.2	100%	90%	94%	88%
	100%	0.8	100%	88%	75%	73%
		1	100%	94%	99%	93%
		1.2	100%	95%	96%	92%
Abnormal combustion process			92.40%	98.50%	98.50%	-7.60%
The ignition process			94.40%	69.10%	69.20%	36.90%
The flameout process			93.00%	97.70%	97.70%	-4.70%

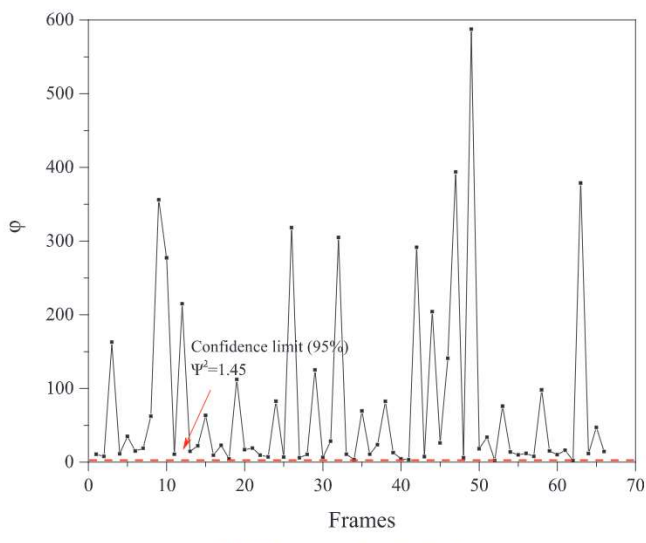
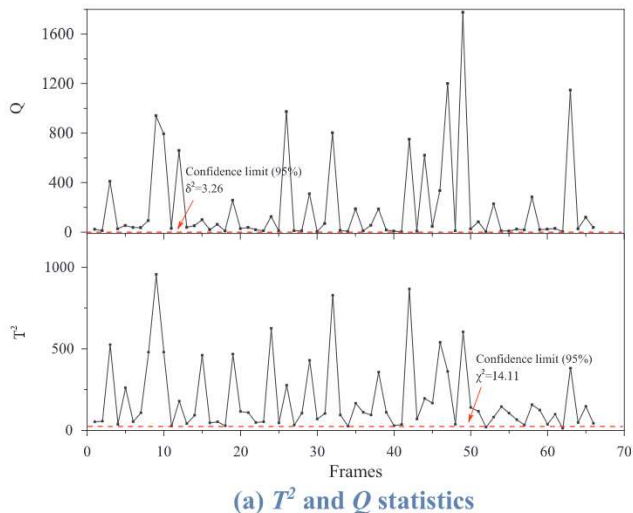


Fig. 9. 66 frames of abnormal gas-fired combustion condition. (a) T^2 and Q statistics (b) Composite statistic.

the ignition process and the flameout process), each of the predication accuracy is not less than 90%, although values of standard deviation are shown to be negative (compared with identification results of composite indicator φ), indicating that high credibility of FPR method has been acquired for the diagnosis of flame states. This performance is evidently better for diagnosing the ignition process (prediction

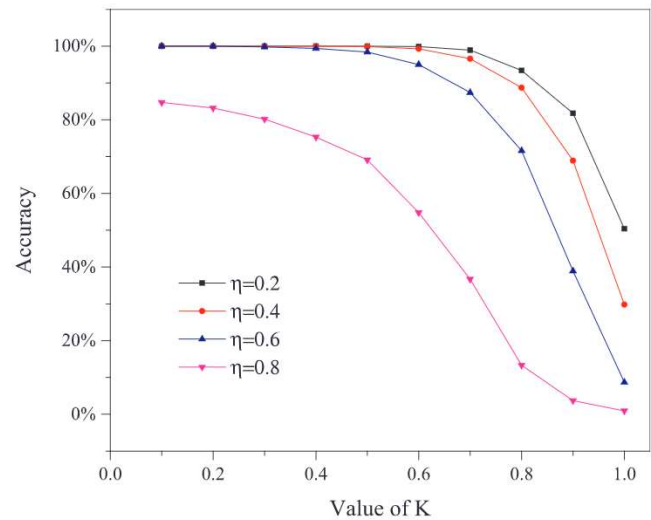


Fig. 10. Prediction accuracy of normal combustion varies with two parameters.

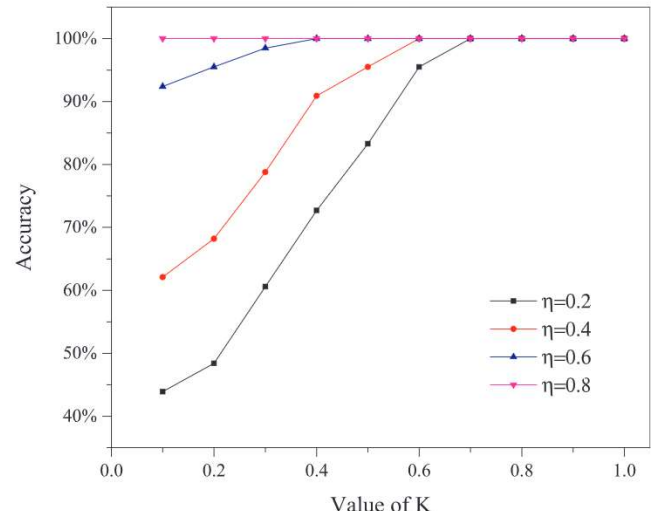


Fig. 11. Prediction accuracy of abnormal combustion varies with two parameters.

accuracy: 94.40%), compared to the assessment results of the selected statistics (displayed in Figs. 8 and 9). Thus, the FPR method established in this study took certain effects, but the robustness of the model was worthy of verification. Figs. 8 and 9 exhibit the diagnosis results of the gas-fired combustion processes (testing case 1 and 2) based on the two statistics and the confidence limit (95%) has been marked with the red

Table 4
Identification results of FPR and other algorithms.

Gas-fired load	Equivalence ratio		Prediction accuracy				
	SOM neural network	SVM	FPR ($\eta = 0.4, k = 0.5$)	FPR ($\eta = 0.5, k = 0.5$)	FPR ($\eta = 0.3, k = 0.6$)		
Normal combustion process	60%	0.8	91%	100%	100%	98%	99%
		1	99%	100%	100%	99%	99%
		1.2	97%	100%	100%	100%	100%
	80%	0.8	100%	100%	100%	100%	100%
		1	100%	100%	100%	100%	100%
		1.2	99%	100%	100%	99%	100%
	100%	0.8	99%	100%	100%	99%	100%
		1	100%	100%	100%	100%	100%
		1.2	98%	100%	100%	100%	100%
Abnormal combustion process			98.48%	96.92%	92.40%	98.48%	98.48%
The ignition process			59.66%	91.46%	94.40%	83.59%	88.26%
The flameout process			97.67%	93.02%	93.00%	93.02%	93.02%

dash line in each figure. The rule of identification here is that if the diagnosis results of both statistics (or a single composite indicator) exceeds confidence limits, a flame state will be considered as an abnormal combustion state.

Next, a sensitivity analysis was conducted for two empirical parameters in FPR model, and to verify the superiority of the proposed method. This study also employed several other algorithms, such as the SOM neural network and SVM, and compared the identification results of them with those from FPR.

Table 4 shows a comparison of the identification results from FPR model and several other algorithms, under different gas-fired loads and equivalence ratios. For normal combustion processes, the numerical instability of SOM neural network (competitive layers: 6×6 , training epoch: 10) is showed in the identification process, and the averaged prediction accuracy is not as good as that of SVM and FPR. Nevertheless, the SOM neural network model shows a good performance in identifying the abnormal combustion process and the flameout process, and the prediction accuracy can reach 97–98%. The results of SVM are good and practical, while its ability to identify the abnormal combustion situation is inferior to that of SOM neural network, providing a reference for further research. The prediction accuracy of the FPR method proposed in this study can be close to that of SVM. For normal combustion, the prediction accuracy of the fuzzy model can reach almost 100%; for abnormal combustion, the ignition process and the flameout process can also achieve a prediction accuracy of more than 90%, and a better prediction accuracy (up to 98%) can be achieved via two-parameter adjustments (especially $\eta = 0.3$, $K = 0.6$).

The FPR method can adjust the two hyper-parameters by experience, gradually improve the prediction accuracy for abnormal combustion, and ensure that the prediction accuracy of normal combustion maintains a high level ($\geq 98\%$). Alternatively, in a case where the prediction accuracy for abnormal combustion has not been significantly lowered, by reducing the value of K or η , the prediction accuracy for normal combustion can be steadily increased.

Assume that the abnormal combustion process and the flameout process are unsteady combustion, the ignition process is a steady combustion; SOM neural network (the competitive layer: 6×6 , training epoch: 10); SVM (based on linear kernel function).

Finally, this study explores the sensitivity of the hyper-parameters to this fuzzy model. In the membership function mentioned before, two empirical scaling factors K and η are used and pre-defined in advance. It was found that both factors had a certain influence on the model results. As can be seen from **Figs. 10** and **11**, the prediction accuracy of normal combustion decreases as η increases when K is kept constant, whereas an opposite trend is presented by the prediction accuracy of abnormal conditions simultaneously. It can be found that, when the value of K is guaranteed to be constant, increasing the value of η can significantly improve the prediction accuracy of an unsteady combustion process, and alternatively, lowering the value of η will increase the prediction accuracy for a normal combustion process. Furthermore, the prediction accuracy for steady combustion is basically 100% ($0.1 \leq K \leq 0.4$), but the prediction accuracy for unsteady combustion is not optimistic. Similarly, the prediction accuracy for unsteady combustion achieve a high level ($0.6 \leq K \leq 1$), whereas the prediction accuracy for steady combustion is at low altitude. In this case, it can be concluded that the sensitivity of the fuzzy model is well-controlled when η is within 0.6, and K is between 0.3 and 0.7.

6. Conclusion

In this study, a four-step pattern recognition method was applied to diagnose flame states in gas-fired combustion. This method has the following advantages. (1) It is often difficult to segment the flame region in a flame image, especially for abnormal combustion of a gas-fired flame. The LEMTS method can solve this problem, and can achieve a good segmentation performance in the flame region. (2) The flame area,

average gray, and other classical flame features cannot well measure the stability of gas-fired flames, and using them for pattern recognition is not very effective. Thus, it is necessary to propose some new features for the flame image, such as the area ratio, connectivity, and rectangular fullness. (3) The FPR method can well-distinguish some gas-fired combustion situations with high similarity. The algorithm is simple and effective, which can identify the normal/abnormal combustion processes of a gas-fired flame, thereby realizing improved online monitoring of gas-fired combustion. (4) The proposed method was trained and tested with numerous data of gas-fired flame image, to ensure the reliability of the identification results. Two statistics (Q and T^2) were used for monitoring of the gas-fired combustion process, and the identification results of the gas-fired flame were also compared using the SOM neural network and SVM algorithm. The results show that the FPR algorithm is superior to these algorithms, and can be further promoted and applied.

CRediT authorship contribution statement

Yu Wang: Conceptualization, Methodology, Software. **Yuefeng Yu:** Investigation, Validation, Visualization. **Xiaolei Zhu:** Data curation, Writing - original draft. **Zhongxiao Zhang:** Writing - review & editing.

Declaration of Competing Interest

The authors declare that they have no known competing financial interests or personal relationships that could have appeared to influence the work reported in this paper.

Acknowledgement

We gratefully acknowledge the financial support provided by National Key Research and Development Project of People's Republic of China (Issue number: 2017YFF0209801).

References

- [1] Ballester J, García-Armengol T. Diagnostic techniques for the monitoring and control of practical flames. *Prog Energ Combust* 2010;36(4):375–411.
- [2] Hernandez R, Ballester J. Flame imaging as a diagnostic tool for industrial combustion. *Combust Flame* 2008;155(3):509–28.
- [3] Jones AR. Flame failure detection and modern boilers. *J Phys E: Sci Instrum* 1988;21(10):921–8.
- [4] Sun D, Lu G, Zhou H, Yan Y. Flame stability monitoring and characterization through digital imaging and spectral analysis. *Meas Sci Technol* 2011;22(11):114007.
- [5] Töreyin BU, Dedeoğlu Y, Güdükbay U, Çetin AE. Computer vision based method for real-time fire and flame detection. *Pattern Recogn Lett* 2006;27(1):49–58.
- [6] Lu G, Yan Y, Colechin M. A digital imaging based multifunctional flame monitoring system. *IEEE Trans Instrum Meas* 2004;53(4):1152–8.
- [7] Muhammad K, Ahmad J, Baik SW. Early fire detection using convolutional neural networks during surveillance for effective disaster management. *Neurocomputing* 2018;288:30–42.
- [8] Bae H, Kim S, Wang B-H, Hyung Lee M, Harashima F. Flame detection for the steam boiler using neural networks and image information in the Ulsan Steam Power Generation Plant 2006.
- [9] Wang J-S, Ren X-D. GLCM based extraction of flame image texture features and KPCA-GLVQ recognition method for rotary kiln combustion working conditions. *Int J Autom Comput* 2015;11(1):72–7.
- [10] Hagan MT, Beale M, Beale M. Neural network design 2002.
- [11] Bishop CM. Neural Networks for Pattern Recognition. *Agr Eng Int Cigr J Scientific Res Develop Manuscript Pm* 1995;12(5):1235–42.
- [12] Sujatha K, Pappa N, Kumar KS, Nambi US. Monitoring power station boilers using ANN and image processing. *Adv Mater Res* 2013;631–632:1154–9.
- [13] Wu X, Kumar V, Quinlan JR, Ghosh J, Yang Q, Motoda H, et al. Top 10 algorithms in data mining. *Knowl Inf Syst* 2008;14(1):1–37.
- [14] Yong BWYJC. A research on application of PCA and SVM to flame monitoring. *Proc CSEE* 2004;24(2):185–90.
- [15] Burges CJC, Smola AJ. Advances in kernel methods: support vector learning. 1999.
- [16] Xuan Truong T, Kim J-M. Fire flame detection in video sequences using multi-stage pattern recognition techniques. *Eng Appl Artif Intell* 2012;25(7):1365–72.
- [17] Zhou H, Tang Q, Yang L, Yan Y, Lu G, Cen K. Support vector machine based online coal identification through advanced flame monitoring. *Fuel* 2014;117:944–51.
- [18] Yiqian WU, Song Y, Zhou H. State identification of boiler combustion flame images

- based on gray entropy multiple thresholding and support vector machine. *Proc Csee* 2013;33(20):66–73.
- [19] Yue HH. Reconstruction-based fault identification using a combined index. *Ind Eng Chem Res* 2001;40(20):4403–14.
- [20] Fukushima K, Neocognitron Miyake S. A self-organizing neural network model for a mechanism of visual. *Pattern Recogn.* 1988.
- [21] Burges CJC. A tutorial on support vector machines for pattern recognition. *Data Min Knowl Disc* 1998;2(2):121–67.
- [22] Lu G, Yan Y, Cornwell S, Whitehouse M, Riley G. Impact of co-firing coal and biomass on flame characteristics and stability. *Fuel* 2008;87(7):1133–40.
- [23] Hirano T. Combustion science for safety. *Proc Combust Inst* 2002;29(1):167–80.
- [24] Yan Y, Lu G, Colechin M. Monitoring and characterisation of pulverised coal flames using digital imaging techniques. *Fuel* 2002;81(5):647–55.
- [25] Huang Y, Yan Y, Lu G, Reed A. On-line flicker measurement of gaseous flames by image processing and spectral analysis. *Meas Sci Technol* 1999;10(8):726–33.
- [26] Molcan P, Gang L, Bris TL, Yong Y, Taupin B, Caillat S. Characterisation of biomass and coal co-firing on a 3 MWth Combustion Test Facility using flame imaging and gas/ash sampling techniques. *Fuel* 2009;88(12):2328–2334.
- [27] González-Cencerrado A, Peña B, Gil A. Coal flame characterization by means of digital image processing in a semi-industrial scale PF swirl burner. *Appl Energy* 2012;94:375–84.
- [28] Chen J, Bao Q. Digital image processing based fire flame color and oscillation frequency analysis. *Procedia Eng* 2012;45:595–601.
- [29] Smart J, Lu G, Yan Y, Riley G. Characterisation of an oxy-coal flame through digital imaging. *Combust Flame* 2010;157(6):1132–9.
- [30] Healey G, Kondepudy R. CCD camera calibration and noise estimation. 1992.
- [31] Gonzalez RC, Wintz P. *Digital image processing*. 2010.
- [32] Shi YH, Eberhart RC. Modified particle swarm optimizer. *Proc IEEE Iccv Conf* 1999.
- [33] Sun D, Lu G, Zhou H, Yan Y. Condition monitoring of combustion processes through flame imaging and kernel principal component analysis. *Combust Sci Technol* 2013;185(9):1400–13.
- [34] Smart J, Gang L, Yong Y, Riley G. Characterisation of an oxy-coal flame through digital imaging. *Combust Flame* 2010;157(6):1132–9.
- [35] Armaselu B, Daescu O. Maximum region rectangle separating red and blue points. *Cccg* 2017.
- [36] Bezdek JC. Pattern recognition with fuzzy objective function algorithms. *Adv Appl Pattern Recog* 1981;22(1171):203–39.
- [37] Dubois BP, Henri. Fuzzy sets and systems: theory and applications. 1980.
- [38] Bezdek JC, Keller J, Krisnapuram R, Pal NR. Fuzzy models and algorithms for pattern recognition and image processing. 2005.
- [39] Shuzi LSDRY. Misfire diagnosis for internal combustion engines using fuzzy pattern recognition. *J Vib Eng* 2000;13(1):37–45.
- [40] Li J, Li X, Tao D. KPCA for semantic object extraction in images. *Pattern Recogn* 2008;41(10):3244–50.
- [41] Qian Z, Sun F, Li W, Liu P. Flame detection using generic color model and improved block-based PCA in active infrared camera. *Int J Pattern Recognit Artif Intell* 2018;32(6):11.